PCCP

Molecular Dynamics Discovery of an Extraordinary Ionic Migration Mechanism in Dislocation-Containing TlBr Crystals

Journal:	*Physical Chemistry Chemical Physics*
Manuscript ID	CP-ART-08-2019-004560.R3
Article Type:	Paper
Date Submitted by the Author:	30-Oct-2019
Complete List of Authors:	Zhou, Xiao Wang; Sandia National Laboratories, Foster, Michael; Sandia National Laboratories, Materials Chemistry Yang, Pin; Sandia National Laboratories Rodriguez, Mark; Sandia National Laboratories, Kim, H.; Radiation Monitoring Devices Cirignano, L. J.; Radiation Monitoring Devices Doty, F.; Sandia National Laboratory,

SCHOLARONE™
Manuscripts

Molecular Dynamics Discovery of an Extraordinary Ionic Migration Mechanism in Dislocation-Containing TlBr Crystals

X. W. Zhou[1], M. E. Foster[2], P. Yang[3], M. A. Rodriguez[4], H. Kim[5], L. J. Cirignano[5],

and F. P. Doty[6]

[1]*Mechanics of Materials Department, Sandia National Laboratories, Livermore, California 94550, USA, Email: xzhou@sandia.gov*

[2]*Materials Chemistry Department, Sandia National Laboratories, Livermore, California 94550, USA*

[3]*Electronic, Optical, and Nano Department, Sandia National Laboratories, Albuquerque, NM 87106, USA*

[4]*Materials Characterization and Performance Department, Sandia National Laboratories, Albuquerque, NM 87106, USA*

[5] *Radiation Monitoring Devices, Watertown, Massachusetts 02472, USA*

[6]*Radiation and Nuclear Detection Materials and Analysis Department, Sandia National Laboratories, Livermore, California 94550, USA*

ABSTRACT

TlBr can surpass CZT for the leading semiconductor for γ- and X- radiation detection. Unfortunately, the optimum properties of TlBr quickly decay when an operating electrical field is applied. Quantum mechanical studies indicated that if this property degradation comes from the conventional mechanism of ionic migration of vacancies, then an unrealistically high vacancy concentration is required to account for the rapid aging of TlBr seen in experiments. In

this work, we have applied large scale molecular dynamics simulations to study effects of dislocations on ionic migration of TlBr crystals under electrical fields. We found that electrical fields can drive the motion of edge dislocations in both slip and climb directions. These combined motions eject enormous vacancies in the dislocation trail. Both dislocation motion and a high vacancy concentration can account for the rapid aging of the TlBr detectors. These findings suggest that strengthening methods to pin dislocations should be explored to increase lifetimes of TlBr crystals.

__Keywords__: molecular dynamics, TlBr crystal, radiation detection semiconductor, structure evolution, ionic migration.

1. INTRODUCTION

TlBr crystals have the desired properties for radiation detection [1,2] including a large band gap (2.7eV), a long carrier lifetime (up to 10^{-4} s), a high average atomic number, and a high resistivity ($\sim 10^{11}$ Ω cm at 298K). As a result, TlBr has demonstrated outstanding performance for room temperature γ-ray detection, reaching resolution $\leq 1\%$ at 662 keV [2,3,4]. This suggests that TlBr can potentially surpass CZT to become the leading semiconductor for radiation detection. However, the performance of TlBr degrades rapidly under operating electrical fields [5,6,7,8,9,10,11,12,13]. Apparently, performance degradation is related to the ionic migration, which leads to a build-up of ions at the electrodes thereby counteracting the applied electrical field and impairing the collection of photo induced carriers. Observation of formation of Tl-rich dendrites near electrodes has also provided direct experimental evidence of ionic migration [6]. Interestingly, however, quantum mechanical studies [14,15,16] indicated that an ionic migration rate that is high enough to account for the rapid aging of TlBr seen in experiments would require

2

a vacancy concentration that is many orders of magnitude higher than the equilibrium vacancy concentration and any excessive vacancy concentrations due to impurities. Therefore, understanding this mysterious, extremely high vacancy concentration becomes relevant to guide future efforts to increase the lifetime of the TlBr devices.

Realistic crystals, especially the soft TlBr crystals, always contain a high density of dislocations due to mechanical deformation. It is unclear if dislocations can promote ionic migration. Here we perform large scale molecular dynamics (MD) to study effects of dislocations on ionic migration under external fields. It should be noted that majority of past MD simulations [17,18,19,20,21,22,23,24] focused on ionic conductivity. As such, the simulations do not apply external electric fields and the systems are simply annealed at sufficiently high temperatures to cause thermally activated diffusion of ions. The diffusion coefficients obtained from the trajectories of ions are then indirectly related to ionic conductivity through Nernst-Einstein equation [25]. Instead, we will apply an external electrical field in MD simulations. Because large systems can be simulated over long time, our studies do not impose any assumptions regarding ionic migration other than introducing dislocations in the system and applying electric fields. As a result, they provide predictions of unknown phenomena. This is also in contrast to quantum mechanical calculations that are typically used to determine the energetics of a pre-assumed mechanism due to the computational cost.

2. METHODS

We apply the molecular dynamics package LAMMPS [26] to perform our simulations. The interatomic forces are modeled by a TlBr polymorphic potential we developed previously [27]. The potential formalism is like that of the widely used Stillinger-Weber potential [28] except that the functions are modified to stabilize the CsCl-type of crystal structure of TlBr as well as to better

capture the energetic transferability between (Tl and Br) elements and (TlBr) compound. There is another TlBr potential available in literature [29], but that potential has only been tested for TlBr melt. The advantage of our potential is that it can predict the crystalline growth of the equilibrium phases of both elements and compounds [27], thereby the equilibrium phases are proven to be more stable than any other low energy configurations that are likely to be all sampled due to random adatom addition during the growth simulations. Potentials with such a validated stability are needed for our simulations where TlBr crystals are required to remain stable with respect to any structural disturbance caused by large electrical fields.

An example of our MD system is showing in Fig. 1. It is a CsCl-type of TlBr crystal containing 60(100) planes in the x direction, 36(010) planes in the y direction, and 56(001) planes in the z direction. Periodic boundary conditions are used in all the three coordinate directions so that the crystal can be viewed as infinitely large. A pair of edge dislocations with a perfect Burgers vector of [100] are created by removing 1(100) plane, or equivalently, 2(200) planes, between a distance d in the y direction. For this paper, d is fixed at 18(010) planes. MD simulations are performed at 800 K using an NVT ensemble (constant number of atoms, volume, and temperature) for a total of 2.02 ns. An external electrical field of E = -0.2 V/Å is simulated by applying a biased force of magnitude of |f| = 0.2 eV/Å, to all the Tl atoms in the –x direction and all the Br atoms in the +x direction, assuming a nominal charge of ±1 electron for Tl and Br atoms. To prevent the crystal from shifting during long time simulations, atoms in a small region near the origin point (0,0,0) are fixed.

Our quantum mechanical calculations [30] confirmed that the main effects of external electric fields are to create a biased force in opposite directions to Tl and Br atoms. These forces can be treated independently from the Coulombic interactions between atoms that are already included in

the interatomic potential. Most importantly, we found that the biased force remains linearly proportional to the applied field up to an extremely high field of 1.5 V/Å, and the charge derived from this linear relationship is not exactly equal to the nominal charge of ±1 electron. Note that the charge derived from force has been termed Born effective charge [31]. While it is interesting that the Born effective charge is not exactly ±1 electron, assuming the nominal charge would at most miss the simulated field by a factor and it should not impact our goal to reveal mechanisms (rather than to derive quantitative relationships).
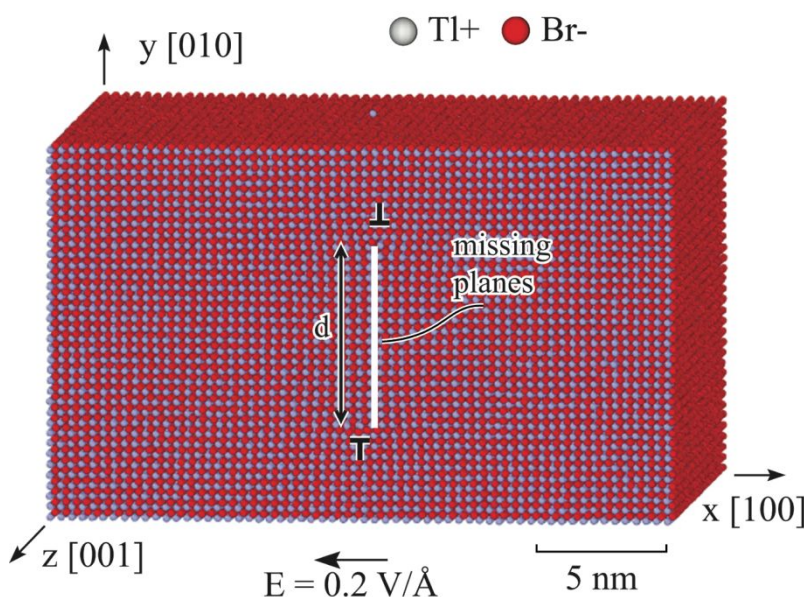
Fig. 1　Geometry of TlBr crystals for molecular dynamics simulations under an electrical field.

3. RESULTS

A.　*Time Evolution of Dislocation Under an Electrical Field*

MD configurations obtained at different times are analyzed using the dislocation extraction algorithm developed and incorporated in the visualization software OVITO by Stukowski [32]. We found that at the absence of any external electrical fields, dislocations remain stationary. However, when a sufficiently large electric field is applied and when the temperature is high

enough to activate the atomic jumps, dislocations move. As an example, Fig. 2 shows OVITO visualization of dislocations obtained from different times at an electrical field of E = 0.2 V/Å and a temperature of T = 800 K. We can see that at the start of simulation, the dislocations are at the original positions as can be confirmed by Fig. 1. At time 0.038 ns, however, the upper dislocation has moved to the left whereas the lower dislocation has moved to the right. With further elapse of time from 0.038 ns to 0.438 ns, Figs. 2(b) – 2(f), the upper dislocation continuously moves to the left. The lower dislocation behaves differently. From 0.038 ns to 0.354 ns, the lower dislocation has moved the entire periodic distance in the right direction, i.e., it has moved out of the right boundary and re-entered from the left boundary before reaching the position shown in Fig. 2(c). Once the lower dislocation reaches the specific location shown in Fig. 2(c), some dislocation segments suddenly change the moving direction, causing the dislocation to bow out. At time 0.370 ns, the left-moving segments become dominant, and the entire dislocation begins to move to the left.

There are additional interesting observations. From 0.370 ns to 0.410 ns, Figs. 2(d) to 2(e), the lower dislocation would have moved the entire periodic distance in the left direction, i.e., the lower dislocation shown in Fig. 2(e) has re-entered from the right boundary. Upon arriving at approximately the same location where the moving direction of the lower dislocation is first reversed, some segments of the lower dislocation would change the moving direction so that the left-moving, lower dislocation suddenly bows out to the right as shown in Fig. 2(e). However, the left-moving dislocation segments always prevail so that eventually the lower dislocation would continuously move to the left, as shown in Figs. 2(e) and 2(f).

In addition to the horizontal motion on the (010) slip plane, the two opposite dislocations are also seen to move vertically in the climb direction. This can be clearly verified in Figs. 2(g) and

6

2(h), where the two dislocations, which were originally separated in the vertical direction, meet

and annihilate.
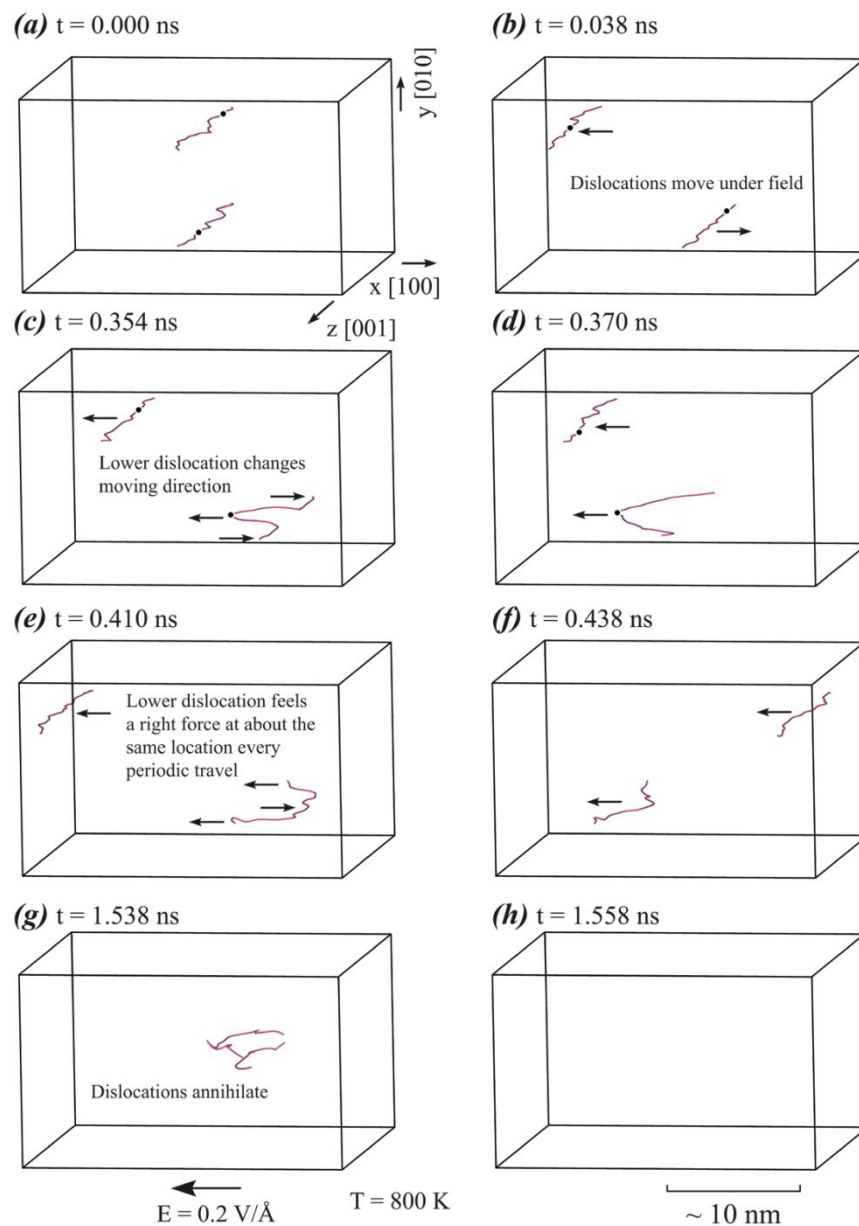
Fig. 2   Dislocation vs. time at a temperature of 800 K and an electrical field of 0.2 V/Å. The black dots on the dislocation lines mark the regions where dislocation cores will be further examined in Fig. 3.

The phenomena observed in Fig. 2 are exciting not only because they can possibly account

for the rapid ionic migration seen in experiments that cannot been accounted for by the

conventional vacancy mechanism, but also because they are truly predicted as we do not impose any assumptions to cause their occurrence. With the phenomena revealed, we will now explore the mechanisms of dislocations migration under electrical fields including thermodynamic origin for the opposite migration of the two dislocations initially and the sudden change of the moving direction of the lower dislocation afterwards. We will also provide a mechanistic understanding as why the lower dislocation always encounters opposite forces and bows out in the opposite direction every time when it moves to the same location where it first changes the moving direction. Finally, we will investigate the details for dislocations climb and any activities of point defects associated with the climb. All these will be presented below.

B. *Dislocation Migration Mechanisms*

To understand the motion of dislocations, the core structures of dislocation segments near the regions marked by the black dots in Fig. 2, are examined in Fig. 3. For perfect CsCl-type of crystal structures examined in the orientation of Fig. 3, each lattice unit (marked by a black line) would contain one atom. Dislocations cores can always be identified as the location where an extra atom (in the projected figures) occurs, i.e., the two atoms (marked by "A" and "B") are present within the lattice unit rather than one atom. At time 0.000 ns shown in Fig. 3(a), for instance, the upper dislocation of the top frame has two Tl atoms A and B occurring within one lattice unit, and the lower dislocation of the bottom frame have two Br atoms A and B within one lattice unit. For convenience, we refer the dislocation with extra Tl atoms at the core to the Tl-rich or α dislocation, and the dislocation with extra Br atoms at the core to the Br-rich or β dislocation. Obviously, dislocation moves only when the leading atoms (marked as "A") at the core make jumps. Under our simulated electrical field, a force in the left direction is applied to the leading Tl atom of the Tl-rich dislocation, and a force in the right direction is applied to the

leading Br atom of the Br-rich dislocation. As a result, the Tl-rich dislocations always move to the left and the Br-rich dislocations always move to the right. This mechanism is confirmed by all the configurations we analyzed including those shown in Figs. 3(b) – 3(d). Specifically, the upper dislocation always moves to the left because its core remains to be Tl-rich as shown in Figs. 3(b) – 3(d). On the other hand, when the lower dislocation moves to the right, it has the Br-rich character at the core as seen in Fig. 3(b). Comparison of Figs. 2(c) and 2(d) with Figs. 3(c) and 3(d) indicates that exactly when the lower dislocation changes the direction of motion, its core transforms from a Br-rich configuration to a Tl-rich configuration. Note that when dislocation core changes, the dislocation must climb by a one atomic plane. Clearly, the charge polarization of dislocation cores is the reason that dislocations in TlBr move under electrical fields, and different polarization (±) is the reason that different dislocations move in different directions.
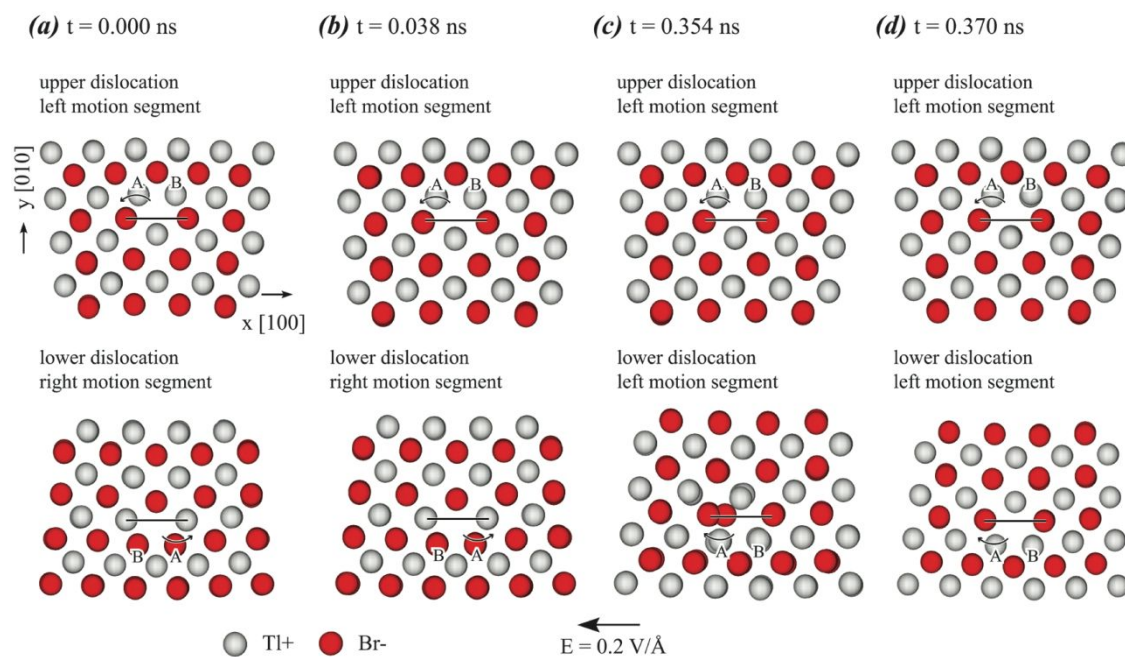
Fig. 3   Examination of dislocation cores at various times.

To understand why the Br-rich dislocation transforms to the Tl-rich dislocation but not the vice versa, we calculate the core energies of both dislocations. As a relative measure, the core energy E_c is simply defined as the average atomic energy for all the atoms within a radius r_0 from the dislocation core. The results of core energies E_c is plotted as a function of r_0 in Fig. 4 for both dislocations. We can see that the Tl-rich dislocation has a lower energy than the Br-rich dislocation over the entire r_0 range explored. This clearly indicates that the Br-rich dislocation is not stable compared to the Tl-rich dislocation. The Br-rich dislocation, therefore, always transforms to a Tl-rich dislocation but not the vice versa.
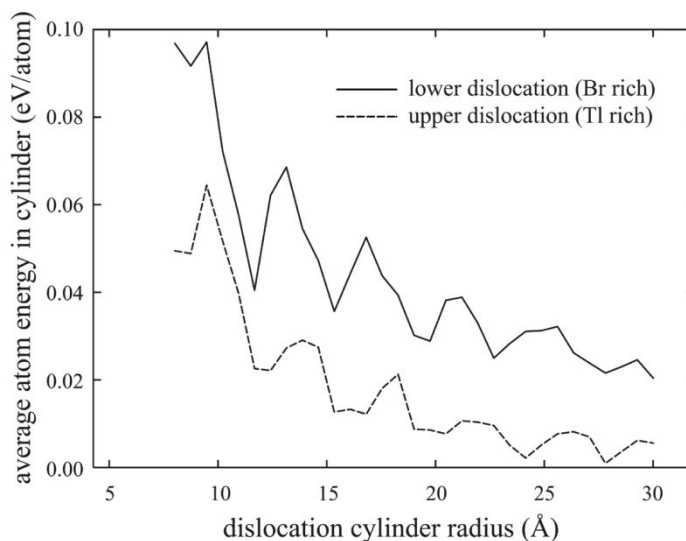
Fig. 4   Core energies of Br-rich and Tl-rich dislocations.

When a dislocation transforms from a Br-rich core to a Tl-rich core, an excess amount of Tl atoms need to be transferred to the core. To understand where these Tl atoms come from, a plan view of two consecutive (010) monolayers adjacent to the slip plane of the lower dislocation right after it changes the moving direction and the core type is examined in Fig. 5. We see that the changes of the dislocation are accompanied by the formation of a large amount of Tl vacancies behind the dislocation. This confirms that a Br-rich dislocation transforms to a Tl-rich

dislocation when a large amount of Tl atoms at the lattice sites jump to the core under the electric field.

Fig. 5 also explains why the lower dislocation encounters an opposite force and bows out every time when it reaches approximately the same location where it first changes the moving direction. This is because this location is associated with a large amount of Tl vacancies. When a Tl-rich dislocation comes close, the excess Tl atoms at the core easily fill these vacancies, resulting in a temporary change of the Tl-rich core to a Br-rich core for some of local segments along the dislocation line. The electrostatic forces acting on these segments then change the sign, and the dislocation then bows out to balance the forces on various segments. However, because the Tl-rich dislocation is more stable than the Br-rich dislocation, the Tl atoms on the lattice sites are gradually dragged back to the core. Eventually the entire dislocation becomes Tl-rich again and therefore continues to move to the left.
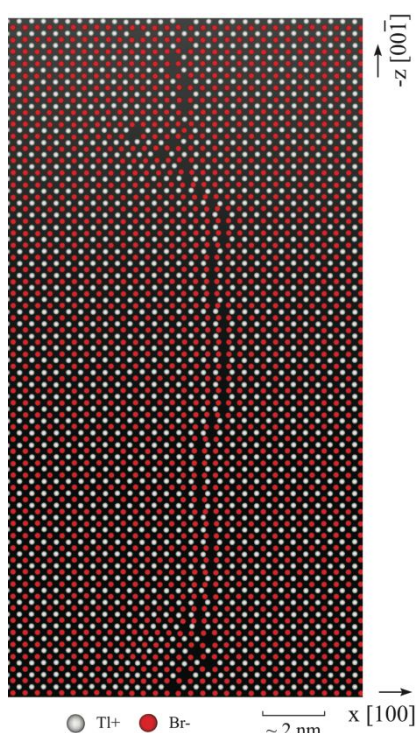
Fig. 5 Plan view of two consecutive (010) monolayers adjacent to the slip plane of the lower dislocation after it changes the moving direction. Significant Tl vacancies are observed.

It should be noted that the motion of both dislocations in the same direction is geometrically necessary. This is because the motion of the upper dislocation in the left direction would cause the shift of the region above the upper dislocation to the left, and the motion of the lower dislocation in the right direction would cause the shift of the region below the lower dislocation to the right. These upper and lower regions are virtually the same region due to the periodic boundary condition, and therefore they cannot shift in the opposite directions. Hence, both dislocations must eventually move in the same direction. One might think that the change of the lower dislocation from a Br-rich core to a Tl-rich core is an artifact of the geometrically necessary condition. This is not the case because once both dislocations became Tl-rich and moved in the same direction at time 0.354 ns, they still continuously climb towards each other. This phenomenon occurred even we significantly increase the y dimension. Fig. 3 indicates that a climb distance of one atomic plane requires the change of dislocation core polarization. Hence, the continuous climb involves alternating switching between Br-rich and Tl-rich dislocation cores, which is not an artifact of the geometrically necessary condition that can be best satisfied when both dislocations remain Tl-rich.

C. *Vacancies Generation Mechanisms*

Migration of point defects is needed for the usual climb motion of edge dislocations. Since the system does not contain point defects initially, the dislocation climb must generate point defects. Three types of point defects, (Tl and Br) interstitials, (Tl and Br) vacancies, and (Tl at Br and Br at Tl) antisites were analyzed. Interstitials can be easily detected because the atomic spacing between an interstitial and the surrounding atoms is abnormally small. Antisites can also be easily detected because an antisite usually have neighbor atoms of the same species (i.e., Tl neighboring Tl and Br neighboring Br) as opposed to different species in bulk TlBr. Based on calculations

using these criteria, we found that concentrations of interstitials and antisites are negligibly small

(occasionally one or two interstitials or antisites occur out of the entire system containing ~240,000

atoms). However, significant vacancies were observed. Hence, we will focus on vacancies.

In a vacancy-free crystal, each Tl atom should have eight Br neighbors and each Br atom

should have eight Tl neighbors. To quantify vacancies, we calculate neighbors of Tl and Br atoms.

If a Tl atom has less than eight Br neighbors, this Tl atom is said to have a neighboring Br vacancy.

Likewise, if a Br atom has less than eight Tl neighbors, it has a neighboring Tl vacancy. The total

number of Tl vacancies is then calculated as 1/8 of the total number of Br atoms that have at least

one neighboring Tl vacancy, and the total number of Br vacancies is calculated as 1/8 of the total

number of Tl atoms that have at least one neighboring Br vacancy. The factor 1/8 arises because

the same, isolated vacancy would have eight atom neighbors. This approach is used to estimate

vacancy density (atomic fraction) as a function of time, and the results are shown in Fig. 6.
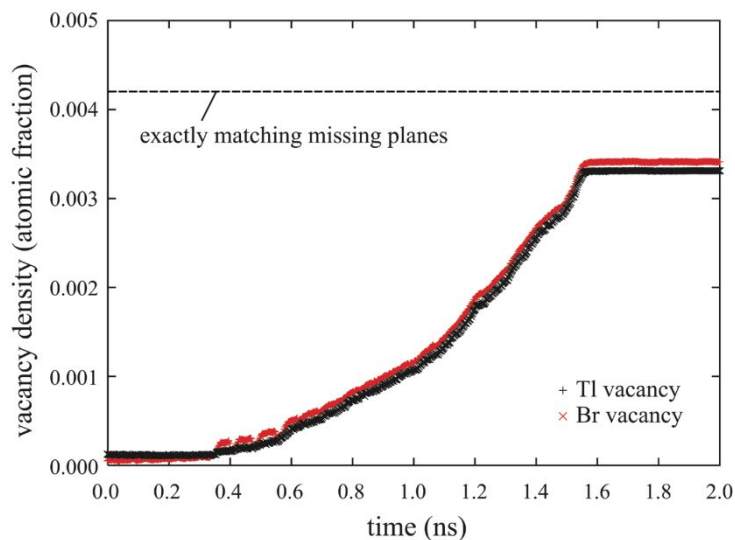
Fig. 6   Tl and Br vacancy concentrations as a function of time.

Fig. 6 shows that vacancy density increases with time until reaches a plateau at around 1.5

to 1.6 ns. Tl ad Br vacancy densities are about the same at all time, satisfying the charge

neutrality condition. The time for reaching the plateau coincides exactly with the time when

13

dislocations annihilate, Figs. 2(g) and 2(h). When dislocations annihilate, the missing planes of

the edge dislocations "disappear" because all the missing atoms are converted to vacancies. The

vacancy density that would match exactly the missing planes is indicated in Fig. 6 using a dash

line. We see that our calculated vacancy density is lower than this ideal vacancy density. This is

correct because when clustered vacancies are formed, an atom can have more than one vacancy

neighbors and a vacancy can have less than eight atom neighbors, both of which cause an

underestimate of vacancy density using our method. Nonetheless, the 0.003 vacancy density

achieved in Fig. 6, would correspond to a vacancy concentration of $\sim 10^{20}$ /cm^3, which can

sufficiently account for the rapid aging seen in experiments [14,15,16].

(a) t = 0.400 ns *(b)* t = 1.200 ns

(c) t = 1.600 ns *(d)* t = 2.000 ns

y [010]

x [100]

○ : dislocation core • : atoms neighboring with Tl vacancies · : atoms neighboring with Br vacancies
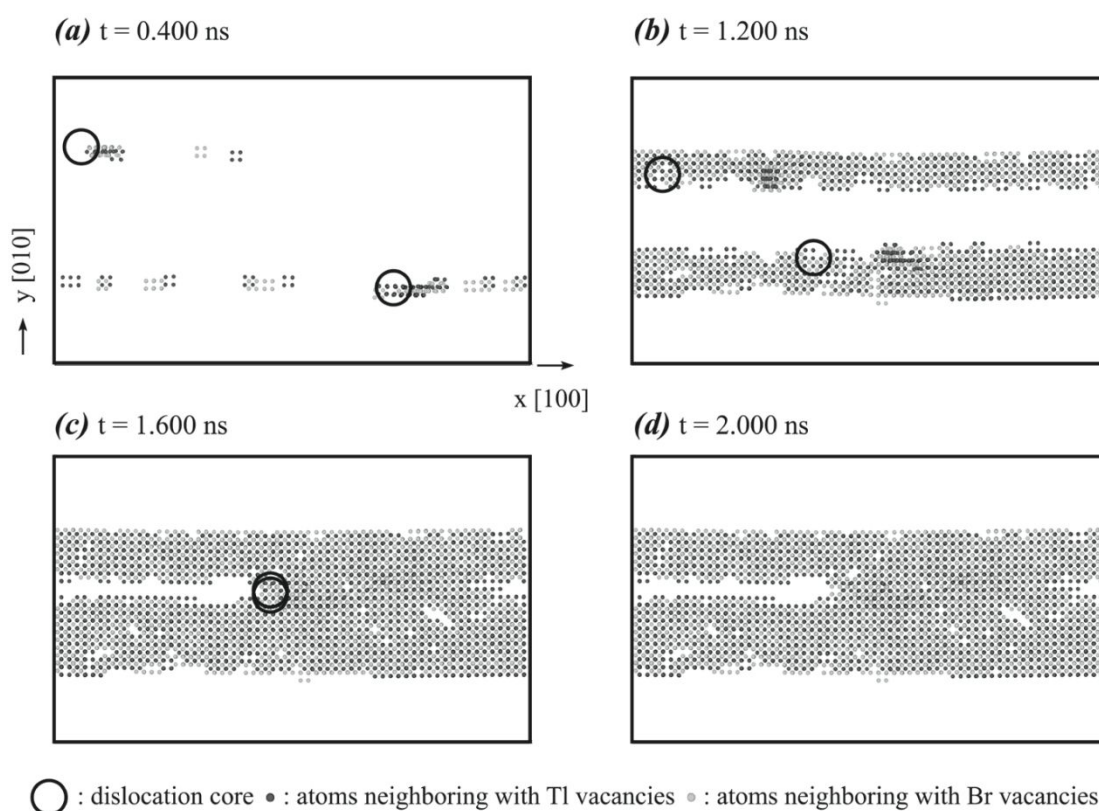
Fig. 7 Vacancy formation mechanisms.

To understand how vacancies are formed, configurations obtained from different times are

visualized in Fig. 7, where only atoms with vacancy neighbors are shown along with the location

14

of dislocation core marked by circles. Fig. 7(a) indicates that at time 0.400 ns where dislocations have moved at least a few periodic lengths (see Fig. 2), there are already quite a few Tl and Br vacancies formed in the trail of the dislocations. Fig. 7(b) indicates that at time 1.200 ns, number of vacancies have increased significantly. Interestingly, whereas the two dislocations are seen to have climbed towards each other for quite a distance, vacancy distribution remains to be continuous (at least in the projected figures) from the original to the current locations of dislocation cores. This suggests that dislocations continuously eject vacancies as they move. According to the discussion above, the climb motion requires atomic jumps from lattice sites to dislocation cores. These jumps will obviously create vacancies in the dislocation trail.

The mechanism discussed above is further verified in Figs. 7(c) and 7(d). Fig. 7(c) corresponds to time 1.6 ns. This is when dislocations meet and annihilate as shown in Fig. 2, and when vacancy densities reach the plateau as shown in Fig. 6. We can see that vacancies are present all the way to the location of dislocation annihilation. Once dislocations are annihilated, no more vacancies are created with a further increase of time to 2.000 ns, Fig. 7(d). Clearly, vacancies are formed due to the climb motion of dislocations.

D. *Implication to Materials Improvement*

Different approaches have been attempted to extend the lifetimes of TlBr, including using biased switching [5], thallium contacts [33], cooling the detectors [34,35], employing various surface treatments [36,37], ultra-purification [2], engineered device geometry [38], optimizing metal contacts [39], and making larger crystals [40]. Although some approaches (e.g., biased switching) are promising, the approaches referred to above are mostly on device engineering rather than material improvements. The MD studies presented above indicate that reducing dislocation density or strengthening materials (reducing dislocation mobility) may be a new

strategy to improve TlBr materials for aging resistance. Numerous ideas can be explored for strengthening. For example, crystallographic orientation engineering to reduce the Schmid factor with respect to the electrical field, grain size refining, aliovalent alloying, precipitate hardening, and work hardening.

4. DISCUSSIONS

A. *Model Approximations*

The 800 K temperature and the 0.2V/Å electrical field used in our MD simulations are both significantly higher than the corresponding 343 K and 0.2×10^{-5} V/Å experimental values [6]. The high temperature and electrical field are necessary to reveal phenomena within the extremely short MD time scales. On the other hand, the interatomic potential defines a melting temperature of 1442 K as compared to the experimental melting temperature of 750 K [27]. We point out that overestimate of melting temperature is necessary for the Stillinger-Weber type of potentials or TlBr crystals would not be stable enough in MD simulations. Given the overestimated melting temperature, it is better to examine the temperature effects based on the homologous temperature. The homologous temperature used in the simulations is 0.55 (= 800/1442), which is to be compared with the corresponding experimental value of 0.46.

To evaluate possibilities of dislocation motion at realistic temperatures and electrical fields, we perform additional simulations at 21 electrical fields 0.10, 0.11, 0.12, …, 0.20 V/ Å, and a fixed temperature, 663 K. We select 663 K because it matches the experimental homologous temperature 0.46 so that we can concentrate on the electrical field. The dislocation migration distance over 2 ns of simulation is shown in Fig. 8. Note that although dislocations do not seem to move at fields ≤ 0.11 eV/Å in Fig. 8, they do move significant distances (e.g., 8.3 nm at 0.10 eV/Å). In fact, we perform one more simulation at 0.02 eV/Å and find a dislocation migration distance of 1.5 nm,

16

which is still not negligible.

Fig. 8 indicates that dislocation velocity is highly statistical, consistent with statistical generation of vacancies. Overall, dislocation velocity decreases with decreasing field. At least in the middle electrical field range shown in Fig. 8, dislocation velocity vs. field relationship seems to be quite linear. This means that at the experimental field, 0.2×10^{-5} V/Å, dislocations might still move considerable distances over application time scales of hours or days. In addition, Fig. 7 clearly shows that dislocation migration velocity is significantly higher than vacancy migration velocity. All these observations suggest that dislocation migration can contribute to the aging under the experimental conditions.
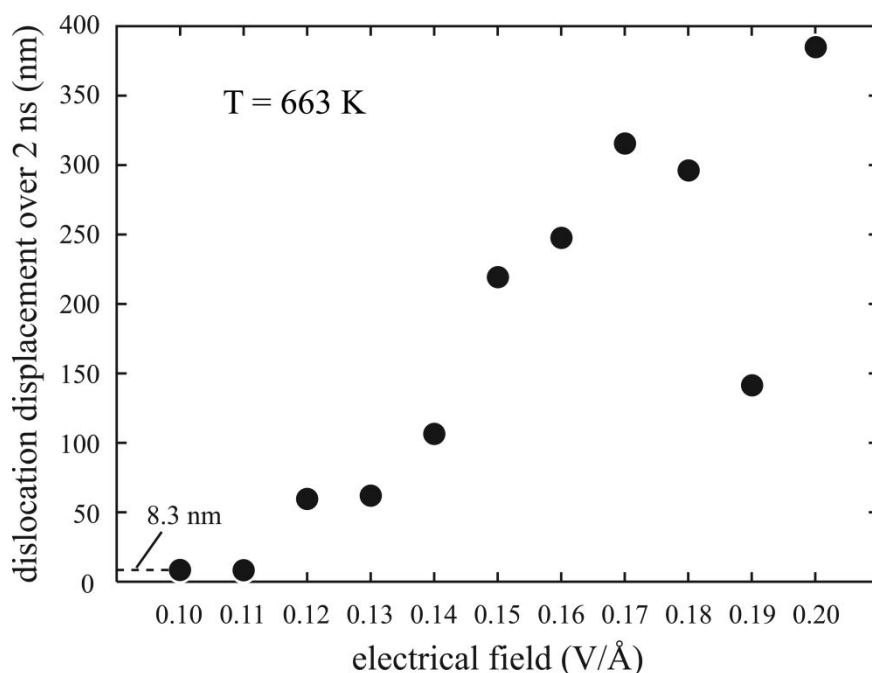
Fig. 8. Dislocation migration distance as a function of electrical field at 663 K.

The use of the periodic boundary condition is another approximation of our MD simulations. First, it prevents build-up of ions at the electrodes counteracting the applied electrical field as seen in experiments. However, this does not impact the initialization of dislocation migration. Furthermore, our purpose is to study if dislocations can facilitate material aging. If the build-up is

severe enough to invalid our simulations, it would already prove that dislocations movement do cause the breakdown of TlBr radiation detectors. Second, the periodic boundary condition requires the use of a dislocation dipole and eventually causes a concerted motion of the two dislocation in the same direction. This approximation does not significantly impact results either because real samples are large and always contains many dislocations. As a result, dislocations can always find other dislocations to engage in concerted motion to meet any geometry requirements.

Note that our simulations do not address the migration of Tl and Br vacancies directly. Our work is based on the previous quantum mechanical calculations [14,15,16] which show that high enough vacancies can lead to the observed rapid aging in the experimental time scale. Our results indicate that electrical fields cause dislocation migration, which in turn creates enormous Tl and Br vacancies. Due to ionic migration, these vacancies are continuously annihilated at contacts, surfaces, and grain boundaries. However, dislocation migrating in a dislocation network microstructure may encounter other dislocations (e.g., forest dislocations) and is therefore pinned at local segments. This creates dislocation multiplication sources such as Frank-Read source [41] and dragging jog source [42]. Because new dislocations can be continuously created, high Tl and Br vacancy densities can be maintained. As a result, the dislocation migration induced vacancies can significantly promote charge separation.

E. CONCLUSIONS

Large scale molecular dynamics simulations have been performed to simulate the effects of dislocations on ionic migration of TlBr crystals under external electrical fields. We found that due to the $\pm$ polarizations of the dislocation cores, Tl-rich (α) and Br-rich (β) dislocations move in opposite directions under a large electrical field. Unlike mechanical deformation induced dislocation motion that is constrained on the slip plane, the electrical field induced dislocation

can move in both slip and climb directions. Due to the climb motion, dislocations eject a large amount of vacancies in their trails. The concentrations of such vacancies can be many orders of magnitude higher than the equilibrium vacancy concentration or impurity induced vacancy concentration. Hence, controlling dislocation density and mobility may be a new strategy to extend lifetimes of TlBr crystals.

F.　CONFLICTS OF INTEREST

There are no conflicts of interest to declare.

G.　ACKNOWLEDGEMENTS

H.　REFERENCES

1　T. E. Schlesinger, J. E. Toney, H. Yoon, E. Y. Lee, B. A. Brunett, L. Franks, and R. B. James, Mater. Sci. Eng., R 32, 103 (2001).
2　A. Churilov, G. Ciampi, H. Kim, L. Cirignano, W. Higgins, F. Olschner, and K. Shah, IEEE Trans. Nuc. Sci., 56, 1875 (2009).
3　K. Hitomi, M. Matsumoto, O. Muroi, T. Shoji, and Y. Hiratate, IEEE Trans. Nuc. Sci., 49, 2526 (2002).
4　M. Shorohov, M. Kouznetsov, I. Lisitskiy, V. Ivanov, V. Gostilo, and A. Owens, IEEE Trans. Nuc. Sci., 56, 1855 (2009).
5　A. Datta, J. Fiala, P. Becla, and S. Motakef, APL Mater., 5, 106109 (2017).
6　A. Datta, P. Becla, and S. Motakef, Nucl. Instrum. Methods Phys. Res. A, 784, 37 (2015).
7　A. Datta and S. Motakef, IEEE Trans. Nucl. Sci., 62, 1244 (2015).

8   K. Hitomi, Y. Kikuchi, T. Shoji, and K. Ishii, IEEE Trans. Nuc. Sci., 56, 1859 (2009).
9   K. Hitomi, T. Shoji, and Y. Nlizeki, Nuc. Instru. Meth. Phys. Res. A, 585, 102 (2008).
10   V. Kozlov, M. Kemell, M. Vehkamaki, and M. Leskela, Nuc. Instru. Meth. Phys. Res. A, 576, 10 (2007).
11   B. Dönmez, Z. He, H. Kim, L. Cirignano, and K. Shah, Nuc. Instru. Meth. Phys. Res. A, 623, 1024 (2010).
12   F. Costa, C. Mesquita, and M. Hamada, IEEE Trans. Nuc. Sci., 56, 1817 (2009).
13   A. Kozorezov, V. Gostilo, A. Owens, F. Quarati, M. Shorohov, M. A. Webb, and J. K. Wigmore, J. App. Phys., 108, 064507 (2010).
14   V. Lordi, J. Cryst. Growth, 379, 84 (2013).
15   C. R. Leaõ, and V. Lordi, Phys. Rev. Lett., 108, 246604 (2012).
16   C. R. Leaõ, and V. Lordi, Phys. Rev. B, 87, 081202(R) (2013).
17   J. X. M. Zheng-Johansson, and R. L. McGreevy, Solid State Ionics, 83, 35 (1996).
18   J. X. M. Zheng-Johansson, I. Ebbsjo, and R. L. McGreevy, Solid State Ionics, 82, 115 (1995).
19   C. W. Huang, W. C. J. Wei, C. S. Chen, and J. C. Chen, J. Euro. Cer. Soc., 31, 3159 (2011).
20   K.-L. Tung, K.-S. Chang, C.-C. Hsiung, Y.-C. Chiang, and Y.-L. Li, Separation Purification Tech., 73, 13 (2010).
21   Y. Yamamura, S. Kawasaki, and H. Sakai, Solid State Ionics, 126, 181 (1999).
22   R. W. J. M. Huang Foen Chung, and S. W. de Leeuw, Solid State Ionics, 175, 851 (2004).
23   J. V. L. Beckers, K. J. van der Bent, and S. W. de Leeuw, Solid State Ionics, 133, 217 (2000).
24   P. J. D. Lindan, and M. J. Gillan, J. Phys.: Condens. Matter, 5, 1019 (1993).
25   R. A. Robinson, and R. H. Stokes, "Electrolyte Solutions" (Academic Press, Inc., New York, 1995).
26   S. Plimpton, J. Comp. Phys., 117, 1 (1995). http://lammps.sandia.gov/.
27   X. W. Zhou, M. E. Foster, Reese Jones, P. Yang, H. Fan, and F. P. Doty, J. Mater. Sci. Res., 4, 15 (2015).
28   F. H. Stillinger, and T. A. Weber, Phys. Rev. B, 31, 5262 (1985).
29   Ç. Tasseven, O. Alcaraz, J. Trullàs, M. Silbert, and A. Giró, J. Phys.: Condens. Matter 9, 11061 (1997).
30   X. W. Zhou, M. E. Foster, P. Yang, and F. P. Doty, MRS Advances, doi: 10.1557/adv.2016.506.
31   X. Gonze, and C. Lee, Phys. Rev. B, 55, 10355 (1997).
32   A. Stukowski, Modelling Simul. Mater. Sci. Eng., 18, 015012 (2010). http://www.ovito.org/.
33   K. Hitomi, T. Shoji, and Y. Nlizeki, Nuc. Instru. Meth. Phys. Res. A, 585, 102 (2008).
34   T. Onodera, K. Hitomi, and T. Shoji, IEEE Trans. Nuc. Sci., 54, 860 (2007).
35   T. Onodera, K. Hitomi, T. Shoji, Nuc. Instru. Meth. A, Phys. Res. A, 576, 433 (2006).
36   I. B. Oliveira, F. E. Costa, P. K. Kiyohara, and M. M. Hamada, IEEE Trans. Nucl. Sci. 52, 2058 (2005).
37   A. M. Conway, L. F. Voss, A. J. Nelson, P. R. Beck, T. A. Laurence, R. T. Graff, R. J. Nikolic, S. A. Payne, H. Kim, L. J. Cirignano, and K. Shah, IEEE Trans. Nuc. Sci., 60, 1231 (2013).

38   V. Gostilo, A. Owens, M. Bavdaz, I. Lisjutin, A. Peacock, H. Sipila, and S. Zatoloka, IEEE
     Trans. Nucl. Sci. 49, 2513 (2002).
39   A. Datta, D. Moed, P. Becla, M. Overholt, and S. Motakef, J. Cryst. Growth, 452, 49
     (2016).
40   H. Kim, L. Cirignano, A. Churilov, G. Ciampi, W. Higgins, F. Olschner, and K. Shah,
     IEEE Trans. Nucl. Sci. 56, 819 (2009).
41   F. C. Frank, and W. T. Read Jr, Phys. Rev., 79, 722 (1950).
42   O. Lohne, and O. Rustad, Philos. Mag., 25, 529 (1972).